Radiology: Imaging Cancer

ORIGINAL RESEARCH

Prospective Evaluation of Whole-Body MRI versus FDG PET/CT for Lesion Detection in Participants with Myeloma

Christina Messiou, FRCR • Nuria Porta, PhD • Bhupinder Sharma, FRCR • Daniel Levine, FRCR • Dow-Mu Koh, FRCR • Kevin Boyd, FRCPath • Charlotte Pawlyn, FRCPath • Angela Riddell, FRCR • Katherine Downey, FRCR • James Croft, FRCPath • Veronica Morgan, MSc • Simon Stern, FRCPath • Betty Cheung, FRCPath • Charalampia Kyriakou, PhD • Pawel Kaczmarek, FRCPath • Jessica Winfield, PhD • Matthew Blackledge, PhD • Wim J. G. Oyen, MD • Martin F. Kaiser, FRCPath

From the Royal Marsden Hospital Foundation NHS Trust, Fulham Rd, London SW3 6JJ, England (C.M., B.S., D.L., D.M.K., K.B., C.P., A.R., K.D., J.C., V.M., S.S., J.W., W.J.G.O., M.F.K.); The Institute of Cancer Research, London, England (C.M., N.P., D.M.K., C.P., J.W., M.B., W.J.G.O., M.F.K.); Epsom and St Helier University Hospitals NHS Trust, Epsom, England (S.S.); Croydon University Hospital, Croydon, England (B.C.); University College London Hospital NHS Foundation Trust, London, England (C.K.); and Surrey and Sussex Healthcare NHS Trust, Redhill, England (P.K.); Received April 24, 2021; revision requested May 18; revision received July 29; accepted August 10. **Address correspondence to** C.M. (e-mail: *Christina.Messiou@rmh.nhs.uk*).

Supported in part by Cancer Research UK (CRUK) and Engineering and Physical Sciences Research Council funding to the Cancer Imaging Centre at the Institute of Cancer Research (ICR) and Royal Marsden Hospital in association with Medical Research Council and Department of Health C1060/A10334, C1060/A16464; National Health Service (NHS) funding to the NIHR Biomedical Research Centre at The Royal Marsden and ICR and the National Institute for Health Research (NIHR) Royal Marsden Clinical Research Facility; and ICR-Clinical Trials and Statistics Unit (ICR-CTSU) core funding from CRUK C1491/A25351. M.K. was supported by a Jacquelin Forbes-Nixon Fellowship

This report is independent research funded by the NIHR. The views expressed in this publication are those of the authors and not necessarily those of the NHS, the NIHR, or the Department of Health.

Conflicts of interest are listed at the end of this article.

Radiology: Imaging Cancer 2021; 3(5):e210048 • https://doi.org/10.1148/rycan.2021210048 • Content codes: CT MR OI

Purpose: To compare disease detection of myeloma using contemporary whole-body (WB) MRI and fluorine 18 (^{18}F) fluorodeoxyglucose (FDG) PET/CT protocols and to correlate imaging with laboratory estimates of disease burden, including molecular characteristics.

Materials and Methods: In this observational, prospective study, participants were recruited from November 2015 to March 2018 who had a diagnosis of myeloma, who were planned to undergo chemotherapy and autologous stem cell transplantation, and who underwent baseline WB-MRI and FDG PET/CT (ClinicalTrials.gov identifier NCT02403102). Baseline clinical data, including genetics, were collected. Paired methods were used to compare burden and patterns of disease.

Results: Sixty participants (mean age, 60 years ± 9 [standard deviation]; 35 men) underwent baseline WB-MRI and FDG PET/CT. WB-MRI showed significantly higher detection for focal lesions at all anatomic sites (except ribs, scapulae, and clavicles) and for diffuse disease at all sites. Two participants presented with two or more focal lesions smaller than 5 mm only at WB-MRI but not FDG PET/CT. Participants with diffuse disease at MRI had higher plasma cell infiltration (percentage of nucleated cells: median, 60% [interquartile range {IQR}, 50%–61%] vs 15% [IQR, 4%–50%]; $P = .03$) and paraprotein levels (median, 32.0 g/L [IQR, 24.0–48.0 g/L] vs 20.0 g/L [IQR, 12.0–22.6 g/L]; $P = .02$) compared with those without diffuse disease. All genetically high-risk tumors showed diffuse infiltration at WB-MRI.

Conclusion: WB-MRI helped detect a higher number of myeloma lesions than FDG PET/CT, and diffuse disease detected at WB-MRI correlated with laboratory measures of disease burden and molecular markers of risk.

Clinical trial registration no. NCT02403102.

Supplemental material is available for this article.

Advances in therapeutics that improve outcomes of patients with myeloma are key drivers for imaging developments. If bone marrow disease is detected early, and patients are treated according to clinical risk, then survival advantages are conferred (1–8). Histologic confirmation of clonal bone marrow plasma cells of greater than 10% in bone marrow or biopsy-proven plasmacytoma is a core requirement of diagnosis that is related to disease burden. However, for a diagnosis of multiple myeloma requiring treatment, biopsy results must be supplemented with evidence of a myeloma-defining event (hypercalcemia, renal failure, anemia, or bone disease) or a biomarker of malignancy (clonal marrow plasma cell percentage ≥ 60%, involved:uninvolved serum free light chain ratio ≥ 100, or a positive finding at MRI) (9). Although the International Myeloma Working Group (IMWG) recommends a range of imaging investigations for bone disease (including low-dose CT, fluorine 18 [^{18}F] fluorodeoxyglucose [FDG] PET/CT, and MRI), the high sensitivity of whole-body (WB) MRI is recognized (10,11), and it is recommended for all patients suspected of having myeloma and who underwent low-dose WB CT or FDG PET/CT with negative findings (12). The IMWG definition of bone involvement as a myeloma-defining event remains the presence of more

Abbreviations

FDG = fluorodeoxyglucose, IMWG = International Myeloma Working Group, IQR = interquartile range, ISS = International Staging System, MY-RADS = Myeloma Response Assessment and Diagnosis System, iTIMM = Image-guided Theranostics in Multiple Myeloma, WB = whole body

Summary

Whole-body MRI had a higher rate of detection of focal and diffuse myeloma compared with fluorodeoxyglucose PET/CT, and diffuse disease was associated with a higher disease burden and high-risk molecular profile.

Key Points

- Whole-body (WB) MRI helped identify at least one focal lesion in 83% (50 of 60) of participants, while fluorine 18 (^{18}F) fluorodeoxyglucose (FDG) PET/CT helped identify at least one focal lesion in 60% (36 of 60) of participants.
- Overall, in 82% (49 of 60) of participants, diffuse disease was detected with WB-MRI, compared to 17% (10 of 60) with FDG PET/CT.
- All genetically high-risk tumors were characterized by diffuse disease infiltration at WB-MRI.

Keywords

MR-Imaging, Skeletal-Appendicular, Skeletal-Axial, Bone Marrow, Hematologic Diseases, Oncology

than one lytic bone lesion larger than 5 mm. However, the updated guidance now includes a positive finding at MRI as a high-risk biomarker. As a consequence, the presence of more than one unequivocal focal lesion in the bone marrow larger than 5 mm can inform decision to treat, and by detecting disease in the marrow space, patients can be treated before cortical bone destruction has occurred (10). In the United Kingdom, WB-MRI is the recommended first-line imaging for all patients suspected of having myeloma, not only because of the relative accuracy, but also because of the benefit of earlier diagnosis on quality of life and survival (13). At present, diffuse disease detected at imaging is not part of the diagnostic paradigm.

Comparisons of MRI and FDG PET/CT have been predominantly retrospective, lacking a reference standard or with inequalities in scan coverage. Although these studies highlighted the sensitivity of MRI, they predate contemporary imaging protocols (14). In particular, WB-MRI has advanced substantially over the last 5 years with the inclusion of diffusion-weighted MRI and Dixon MRI, which contribute to increasing accuracy and quantitative capabilities (15–17). Unfortunately, MRI studies that have not included diffusion-weighted sequences cannot reliably distinguish active from inactive sites and are prone to false-positive findings. One recent prospective study (18) compared WB-MRI, including diffusion-weighted MRI, with FDG PET/CT, and WB-MRI was found to have a higher sensitivity for detecting focal bone lesions. Hence, further confirmation of WB-MRI with diffusion-weighted MRI as a staging tool in myeloma will help to establish its wider deployment in clinical practice.

Although focal lesion detection is crucial for decision making, burden of disease at MRI and FDG PET/CT also has prognostic implications. The number of lesions is related to overall and event-free survival (19), and accurate assessment of burden may facilitate risk stratification beyond current diagnostic criteria. The impact of direct visualization and potential quantification of disease burden at WB imaging becomes even more compelling when considering that current biomarkers of burden such as paraprotein, light chains, and albumin are indirect. WB imaging has also highlighted vulnerabilities in percentage of plasma cell infiltration at bone marrow biopsy as a direct measure of disease burden, as heterogeneous disease distribution and sampling errors can lead to underestimation, but also overestimation, of disease burden (20).

In addition to assessment of disease burden, bone marrow tumor genetics including immunoglobulin locus translocations t(4;14), t(14;16), and t(14;20) and copy number aberrations del(1p), gain(1q), and del(17p) are markers associated with adverse prognosis in myeloma (21). Their assessment is recommended for all patients at diagnosis for stratification of patient management (21). However, in addition to a degree of variability due to heterogeneous disease distribution and sampling errors, there is substantial variability in access to and quality of testing for these markers (22,23). The development of radiomic markers could therefore potentially facilitate patient stratification.

To address these uncertainties and define the role of WB-MRI in myeloma, we conducted a prospective study to compare the detection of focal and diffuse disease using WB-MRI and FDG PET/CT protocols. We also investigated correlation of imaging assessments with serum and marrow estimates of disease burden, as well as molecular disease characteristics, to establish the value of WB-MRI as a staging tool in myeloma.

Materials and Methods

Trial Design

We conducted a single-center observational study of baseline WB-MRI and FDG PET/CT in prospectively recruited participants with either a new diagnosis of symptomatic multiple myeloma or at first relapse, who were planned to undergo induction therapy and high-dose melphalan and autologous stem cell transplant, respectively, with WB-MRI follow-up at 3 months and 2 years after autograft (Image-guided Theranostics in Multiple Myeloma [iTIMM] study, ClinicalTrials.gov identifier NCT02403102). We report here on preplanned baseline comparison of WB-MRI and FDG PET/CT. Institutional review board and national ethics committee approval were obtained. Written informed consent was obtained from all participants. Participants were recruited between November 11, 2015, and March 3, 2018.

Participant Sample

Inclusion criteria were age of 18 years or older, a new diagnosis of multiple myeloma or disease at first relapse, and planned for high-dose melphalan and autologous stem cell transplant. Diagnosis and relapse were defined as per IMWG criteria using laboratory parameters including bone marrow trephine biopsy and assessment of end-organ damage (9,24).

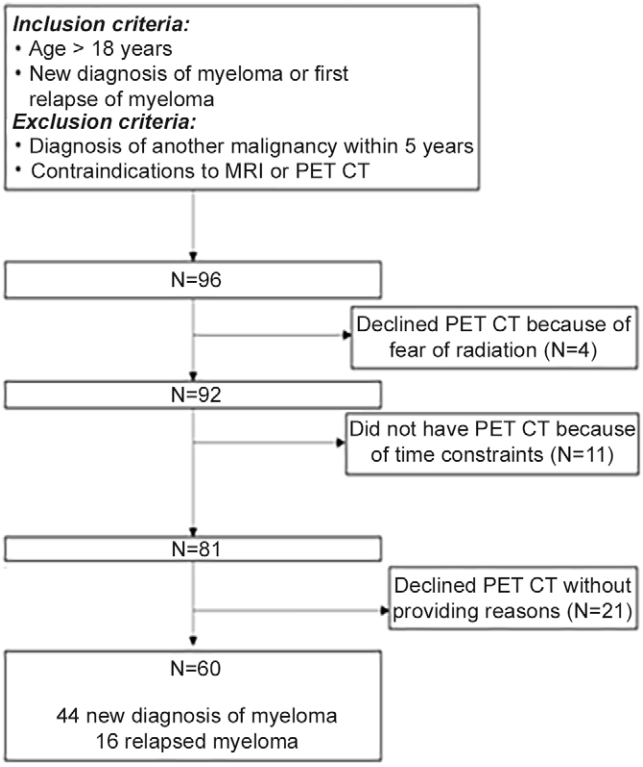

Figure 1: Trial flow diagram illustrating selection criteria, initial participants, and exclusions.

Participants with a diagnosis of another malignancy in the prior 5 years or contraindications to MRI or FDG PET/CT were excluded. WB-MRI and FDG PET/CT were performed within 7 days of one another. Figure 1 shows a flowchart of participant inclusion.

MRI Protocol

WB-MRI was performed using a Siemens Avanto 1.5-T system in line with the Myeloma Response Assessment and Diagnosis System (MY-RADS) consensus document (15), which provides guidelines for acquisition, interpretation, and reporting of WB-MRI for patients with myeloma. T1-weighted and T2-weighted sagittal spine images were acquired, followed by axial diffusion-weighted sequences covering head to knees and axial three-dimensional gradient-echo Dixon sequences. Sequence parameters are summarized in Table 1. Average total acquisition time was 45 minutes.

FDG PET/CT Protocol

PET/CT images were acquired using the radiopharmaceutical FDG, all participants being in a fasted state. The administered FDG dose varies according to the weight of the participant and is calculated as per the European Association of Nuclear Medicine Linear Scheme. Scans were performed with Biograph mCT 64- and 128-section and Biograph Horizon 16-section PET/CT scanners (Siemens Healthineers), images acquired 60 minutes after FDG injection, with total body scans vertex to feet and 2 minutes per bed position.

Clinical Data Collection

Baseline clinical data of presentation at trial entry (new diagnosis or relapse), laboratory markers (β_2-microglobulin, albumin, platelet, hemoglobin, calcium, lactate dehydrogenase, creatine, serum free light chains and ratio, serum paraprotein, bone marrow cellularity and infiltration at trephine and aspirate biopsies, urinary Bence Jones protein), and tumor assessments and genetics (translocations and abnormalities) were collated into an anonymized database.

Image Analysis

WB-MRI and FDG PET/CT scans were scored by two blinded experienced reporting radiologists (A.R., K.D.) and two nuclear medicine physicians (B.S., D.L.) (more than 10 years of experience each), respectively, and a final score was achieved by consensus. Discrepant cases were brought back to the readers for consensus by a third independent reader (C.M. for WB-MRI, W.J.G.O. for FDG PET/CT, each with more than 10 years of experience). Disease burden was scored as previously published: dependent on number and size of lesions and presence of diffuse disease (17). For each of seven skeletal sites (skull, cervical spine, thoracic spine, lumbar spine, pelvis, long bones, ribs, and others [including clavicles, sternum, and scapulae]), a score was computed by the sum of the score for number of lesions (3 for >10 lesions, 2 for ≥five lesions but <10, and 1 for one to four lesions) and the score for size of largest lesions (3 for >20 mm, 2 for 10–20 mm, and 1 for <10 mm) (25). The presence of diffuse disease at each site was documented. A total score was calculated as the sum of all sites.

Focal and diffuse disease at MRI were defined as per the MY-RADS criteria (15). Focal lesions were defined as hyperintense to background muscle at a *b* value of 900 sec/mm^2 (*b*900), excluding T2 shine-through, using apparent diffusion coefficient maps and confirming the presence of focal lesions using corresponding Dixon sequences. Diffuse disease was documented where bone marrow returned higher signal than muscle at *b*900 sec/mm^2. At FDG PET/CT, focal lesions were defined as focal bone destruction of greater than 5 mm with or without FDG uptake if it was higher than background marrow, not explained by findings at CT, such as degenerative change or fractures. Diffuse disease was documented where background marrow FDG uptake was greater than that of the liver (26,27). It is acknowledged that due to potential false-positive findings, diffuse disease must be supported by bone marrow trephine biopsy (bone marrow core biopsy from the posterior iliac crest), which was part of the diagnostic criteria for inclusion in the study (15) (Figs 2–5).

For both WB-MRI and FDG PET/CT, focal disease and diffuse disease can coexist and are not mutually exclusive.

Statistical Analysis

The sample size of 60 participants was determined for the primary endpoint in the iTIMM trial: diagnostic accuracy of disease burden score at 3 months after autologous stem cell transplantation to predict disease status at 2 years. For the baseline comparison of paired WB-MRI and FDG PET/CT total disease burden scores presented in this report, 60 participants would al-

Table 1: Whole-Body MRI Sequence Parameters

Parameter	T1-weighted Spine Imaging	T2-weighted Spine Imaging	Diffusion-weighted Imaging	Gradient-Echo Dixon Imaging
Sequence	TSE	TSE	EPI	3D gradient echo (FLASH)
Section orientation	Sagittal	Sagittal	Axial	Axial
No. of stations	2	2	6	6
Section thickness (mm)	4	4	5	5
Sections per station	15	15	50	40
Field of view (read) (mm)	400	400	430	430
Acquired matrix (read)	448	512	140	256
Reconstructed matrix (read)	448	512	280	512
Reconstructed pixel size (mm)	0.9 × 0.9	0.8 × 0.8	1.5 × 1.5	0.8 × 0.8
TE (msec)	11	83	66	2.38 and 4.76
TR (msec)	683	3110	14500	7.1
Flip angle (degree)*	150	150	90	15
Receiver bandwidth (Hz/pixel)	215	191	1984	400
Parallel imaging	GRAPPA factor 2	GRAPPA factor 2	GRAPPA factor 2	GRAPPA factor 3
Fat suppression	None	None	STIR (TI = 180 msec)	Dixon
b Value (sec/mm^2)	NA	NA	50, 900	NA
Diffusion gradient scheme	NA	NA	bipolar	NA
Diffusion mode	NA	NA	3-scan trace	NA
No. of signal averages	1	1	4	1
Breathing instructions	Free breathing	Free breathing	Free breathing	Breath hold
Acquisition time per station	1 minute 36 seconds	1 minute 22 seconds	6 minutes 11 seconds	17 seconds

Note.—EPI = echo-planar imaging, FLASH = fast low-angle shot, GRAPPA = generalized autocalibrating partially parallel acquisition, NA = not applicable, STIR = short-tau inversion recovery, TE = echo time, TI = inversion time, TR = repetition time, TSE = turbo spin echo, 3D = three dimensional.
*Flip angle: refocusing angle is quoted for TSE; excitation angle is quoted for EPI and FLASH sequences.

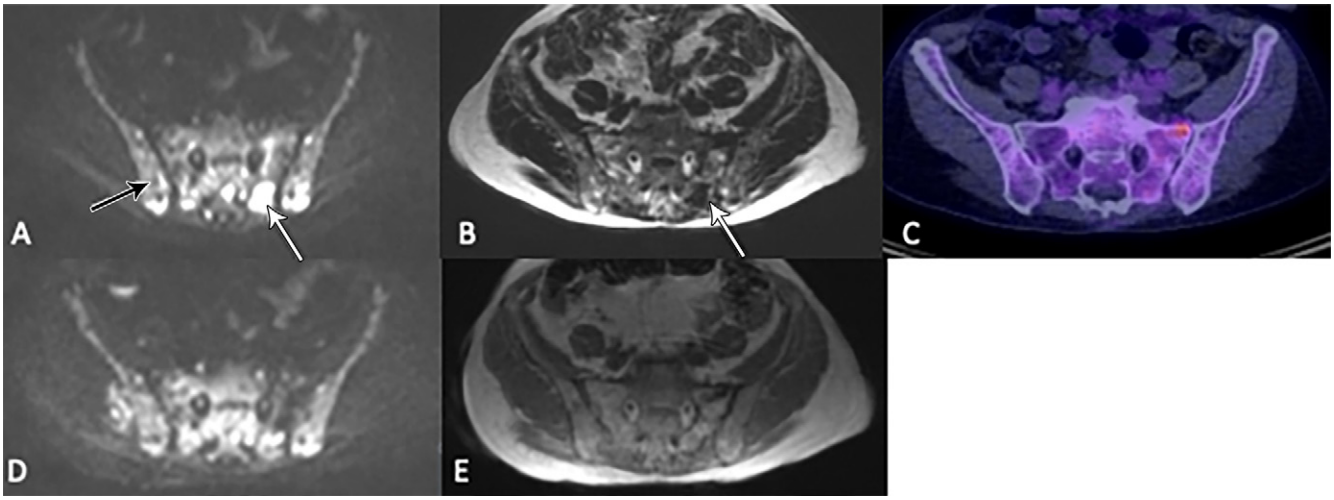

Figure 2: Images in a 67-year-old woman show posttreatment resolution of a lesion detected at whole-body MRI but not PET/CT, thereby ruling out a false-positive finding. **(A)** A focal lesion within the left posterior sacrum seen at axial *b*900 diffusion-weighted imaging (white arrow) and **(B)** Dixon T1-weighted imaging (arrow) was observed at **(C)** corresponding fluorine 18 fluorodeoxyglucose PET/CT (50% bone marrow infiltration by myeloma cells; IgG λ paraprotein, 62 g/L; serum free κ light chains, 6 mg/L; λ light chains, 47 mg/L; light chain ratio, 0.13). Increased signal from background marrow (black arrow in **A**) relative to muscle also suggested diffuse infiltration that was not detected at PET/CT. **(D)** Axial *b*900 diffusion-weighted image after chemotherapy and **(E)** Dixon T1-weighted image show the lesion had resolved. (At time of scan, there was < 1% bone marrow infiltration; paraprotein, 2 g/L; κ light chains, 9 mg/L; λ light chains, 6 mg/L; and light chain ratio, 1.5; participant reached immunofixation-negative complete remission a few months later without further intervention).

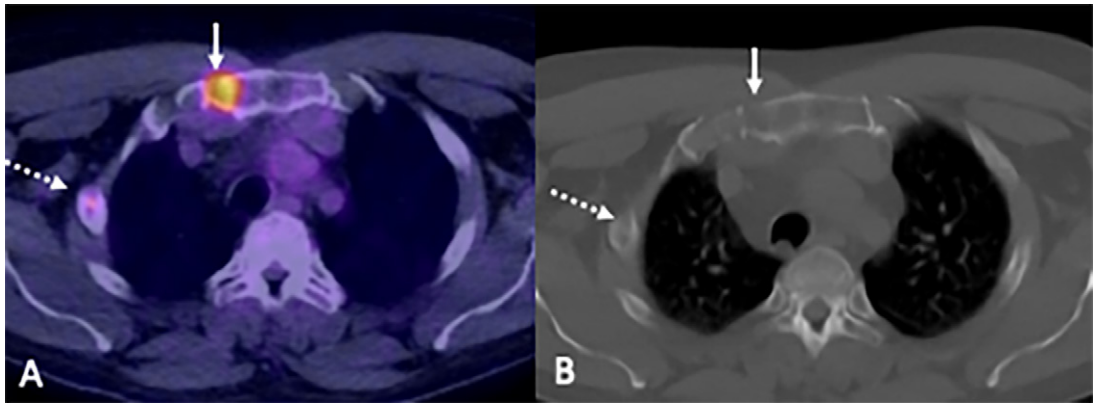

Figure 3: Images in a 54-year-old man show disease detection at fluorine 18 fluorodeoxyglucose (FDG) PET/CT. **(A)** Focal increased FDG uptake (solid arrow) corresponds with bone destruction on the CT-only image. **(B)** A second subtle rib lesion was also observed (dashed arrow) (10% bone marrow infiltration by myeloma cells; paraprotein not detectable; serum free κ light chains, 14 mg/L; λ light chains, 1820 mg/L; light chain ratio, 0.01).

low the detection of an effect size of at least 0.4 with greater than 80% power and 5% α.

Analysis was conducted using Stata version 15. All participants who underwent baseline WB-MRI and FDG PET/CT were included in the analysis. For the total score, missing assessments at a specific site were considered zero and the site thus included in the overall score. Therefore, if a lesion was found and scored at WB-MRI but not found at FDG PET/CT, the score for that site was 0 for FDG PET/CT. Percentages of agreement or disagreement were computed over the total of participants with paired scans. Differences between WB-MRI and FDG PET/CT for quantifying burden and patterns of disease were tested with McNemar test, Bowker symmetry test, and Wilcoxon signed rank test for paired binary, ordinal, and continuous features, respectively. To quantify the agreement between total disease burden score at WB-MRI and FDG PET/CT, Lin concordance index was computed. Differences within specific sites were similarly analyzed, but post hoc tests using Holm correction to adjust *P* values were performed to account for multiplicity. A significance level of .05 was used.

To investigate the association of WB-MRI and FDG PET/CT assessments with laboratory parameters, we compared these features within exclusive groups resulting from classifying participants according to focal disease (negative or positive for both or either WB-MRI and FDG PET/CT) and presence of diffuse disease (yes or no). Methods to compare two or more independent groups were used: nonparametric Wilcoxon rank sum test (for two-group comparisons) or Kruskal-Wallis test (for more than two–group comparisons) for numeric features, χ^2 or exact tests for categorical variables.

Results

Participant Sample

Ninety-six consecutive participants were eligible for enrollment; however, four participants declined FDG PET/CT due to participant concerns regarding radiation exposure, 11 participants could not undergo FDG PET/CT due to insufficient time for two scans prior to treatment date, and a further 21 participants declined FDG PET/CT without a reason given. No participants declined study participation on the basis of MRI. Therefore 60 participants (mean age, 60 years ± 9; 35 men) underwent baseline WB-MRI and FDG PET/CT after enrollment into the iTIMM trial, of which 73% (44 of 60) of participants had a new diagnosis of myeloma, and 27% (16 of 60) were imaged at first relapse (Fig 1). No studies were excluded due to suboptimal image quality. The median time between WB-MRI and FDG PET/CT was 0 days (interquartile range [IQR], 0–6.5 days). Only one participant (1.7%) had extramedullary disease (pancreatic and subcutaneous) that was detected with both modalities. Participant demographics and baseline features are summarized in Table 2.

Concordance between WB-MRI and FDG PET/CT for Focal and Diffuse Disease

Focal disease.— WB-MRI depicted at least one focal lesion in 83% (50 of 60) of participants, while FDG PET/CT depicted at least one focal lesion in 60% (36 of 60) of participants (Figs 2, 3). In all participants with focal lesions detected with FDG PET/CT, these same focal lesions were also detected with WB-MRI. There were 17% (10 of 60) of participants who did not present with any focal disease (either at WB-MRI or FDG PET/CT), 60% (36 of 60) who presented focal disease at both WB-MRI and FDG PET/CT, and 23% (14 of 60) of participants who presented with focal disease at WB-MRI but not at FDG PET/CT (Fig 4, Table 3). For participants without focal disease at FDG PET/CT (*n* = 24), WB-MRI depicted predominantly (46%; 11 of 24) a small number of focal lesions (one to four). However, close to 13% (three of 24) of these participants presented with five or more focal abnormalities at WB-MRI (Table 3, Fig 4). Accordingly, concordance between WB-MRI and FDG PET/CT for depiction of focal lesions was low, ranging from 52% for dorsal spine and long bones to 78% for skull (Table E1 [supplement]). Discordance was significant for long bones (*P* = .007), lumbar spine (60%; *P* = .04), and pelvis (57%; *P* = .02). All additional lesions identified at WB-MRI, compared with FDG PET/CT (*n* = 14), resolved following treatment.

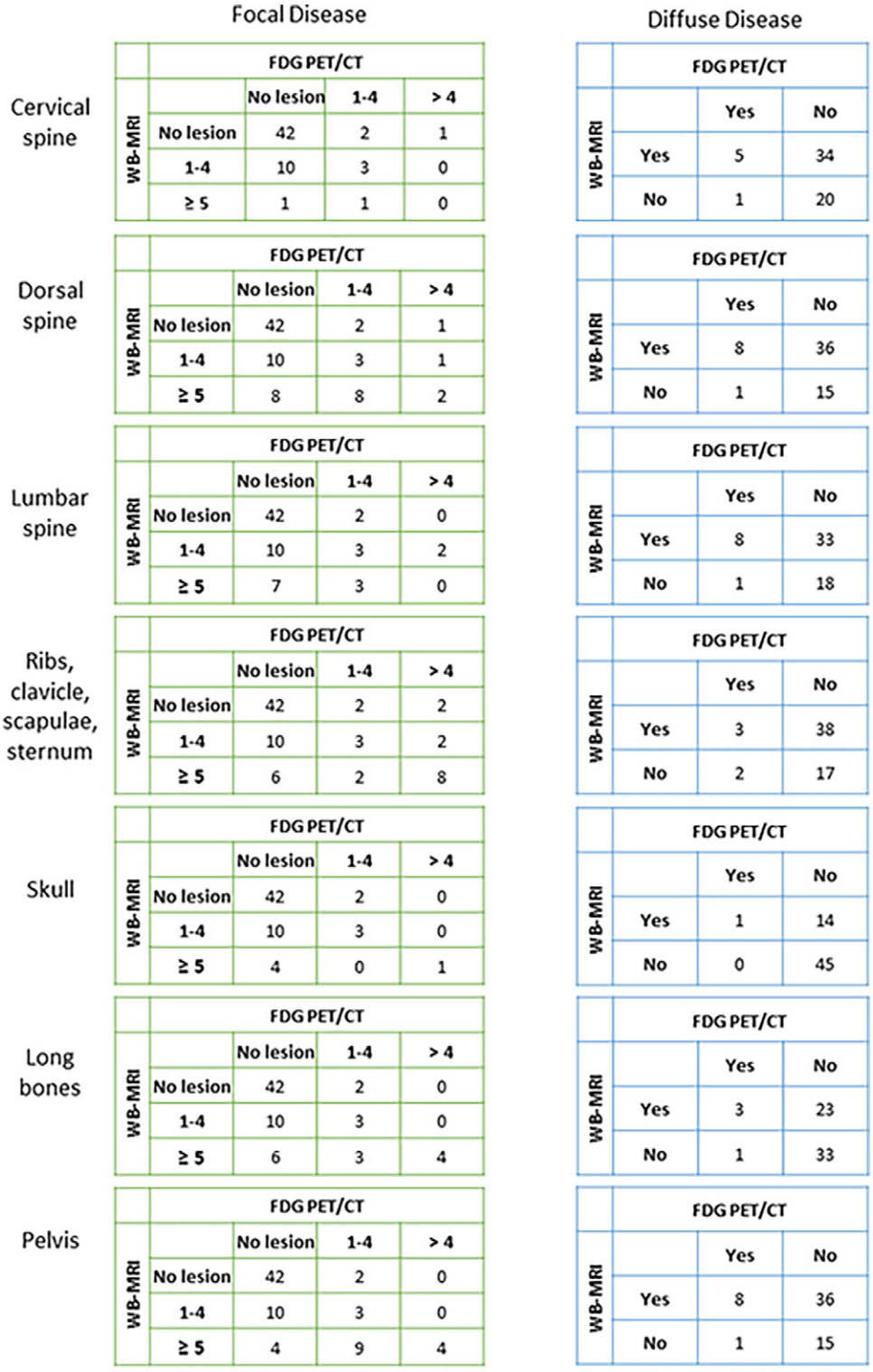

Cervical spine	FDG PET/CT: No lesion	1-4	> 4
WB-MRI: No lesion	42	2	1
WB-MRI: 1-4	10	3	0
WB-MRI: ≥ 5	1	1	0

Cervical spine	FDG PET/CT: Yes	No
WB-MRI: Yes	5	34
WB-MRI: No	1	20

Dorsal spine	FDG PET/CT: No lesion	1-4	> 4
WB-MRI: No lesion	42	2	1
WB-MRI: 1-4	10	3	1
WB-MRI: ≥ 5	8	8	2

Dorsal spine	FDG PET/CT: Yes	No
WB-MRI: Yes	8	36
WB-MRI: No	1	15

Lumbar spine	FDG PET/CT: No lesion	1-4	> 4
WB-MRI: No lesion	42	2	0
WB-MRI: 1-4	10	3	2
WB-MRI: ≥ 5	7	3	0

Lumbar spine	FDG PET/CT: Yes	No
WB-MRI: Yes	8	33
WB-MRI: No	1	18

Ribs, clavicle, scapulae, sternum	FDG PET/CT: No lesion	1-4	> 4
WB-MRI: No lesion	42	2	2
WB-MRI: 1-4	10	3	2
WB-MRI: ≥ 5	6	2	8

Ribs, clavicle, scapulae, sternum	FDG PET/CT: Yes	No
WB-MRI: Yes	3	38
WB-MRI: No	2	17

Skull	FDG PET/CT: No lesion	1-4	> 4
WB-MRI: No lesion	42	2	0
WB-MRI: 1-4	10	3	0
WB-MRI: ≥ 5	4	0	1

Skull	FDG PET/CT: Yes	No
WB-MRI: Yes	1	14
WB-MRI: No	0	45

Long bones	FDG PET/CT: No lesion	1-4	> 4
WB-MRI: No lesion	42	2	0
WB-MRI: 1-4	10	3	0
WB-MRI: ≥ 5	6	3	4

Long bones	FDG PET/CT: Yes	No
WB-MRI: Yes	3	23
WB-MRI: No	1	33

Pelvis	FDG PET/CT: No lesion	1-4	> 4
WB-MRI: No lesion	42	2	0
WB-MRI: 1-4	10	3	0
WB-MRI: ≥ 5	4	9	4

Pelvis	FDG PET/CT: Yes	No
WB-MRI: Yes	8	36
WB-MRI: No	1	15

Figure 4: Focal and diffuse disease detection with whole-body (WB MRI versus fluorine 18 fluorodeoxyglucose (FDG) PET/CT per anatomic region. For each anatomic region, separate cross tables detail number of participants with focal disease (subgrouped by number of lesions) or diffuse disease detected with WB-MRI or FDG PET/CT.

Diffuse disease.— All participants without focal disease (n = 10) presented with diffuse disease at WB-MRI (100%), but only four of these (40%) presented with diffuse disease at FDG PET/CT. Diffuse disease was frequently detected at WB-MRI across all anatomic sites (Fig 5A; Table 3, Table E2 [supplement]). Overall, for 82% (49 of 60) of participants, diffuse disease was detected with WB-MRI, compared with 17% (10 of 60) with FDG PET/CT (Figs 5, 6, Table 3). For participants with focal disease detected with either WB-MRI or FDG PET/CT, 83% (50 of 60) were also found to have diffuse infiltration with WB-MRI compared with 17% (10 of 60) with FDG PET/CT (Fig 7A). Concordance between detection of diffuse disease with WB-MRI or FDG PET/CT was low and ranged from 33% for ribs to more than 38% for areas containing larger volumes of bone marrow space, such as dorsal spine or pelvis, to 76% in the skull (Table E2 [supplement]).

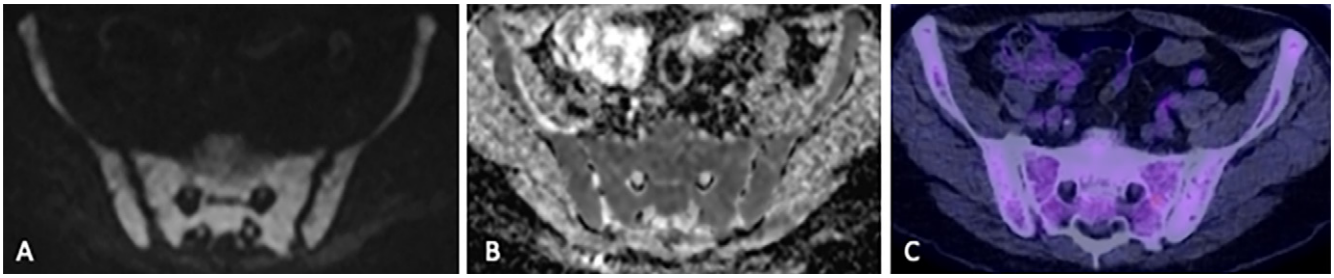

Figure 5: Images in a 71-year-old man show diffuse infiltration detected at MRI but not fluorodeoxyglucose (FDG) PET/CT. **(A)** Diffuse increased signal throughout the pelvic bone marrow relative to background tissue on axial *b*900 diffusion-weighted image and intermediate apparent diffusion coefficient (638 mm^2/sec) on the **(B)** apparent diffusion coefficient map indicates diffuse hypercellularity, suggesting diffuse infiltration. However, **(C)** the corresponding FDG PET/CT image did not show an abnormality. Bone marrow sampling confirmed 85% infiltration of the bone marrow by myeloma.

Table 2: Participant Demographics and Laboratory Features

Parameter	Value
No. of participants	60 (100)
No. of men	35 (58)
Age (y)	60 ± 9
Presentation at trial entry	
Newly diagnosed	44 (73)
Pre-existing MGUS*	3 (6.8)
Pre-existing asymptomatic MM*	6 (14)
Relapse	16 (27)
Received induction therapy before first ASCT†	16 (100)
Cyclophosphamide, thalidomide, dexamethasone	13 (81)
Cyclophosphamide, bortezomib, dexamethasone	1 (6)
Cyclophosphamide, bortezomib, thalidomide	1 (6)
Cyclophosphamide, bortezomib, thalidomide, dexamethasone	1 (6)
No. of induction cycles, median	4 (4–5)
Received maintenance therapy	0
Months to progression from first ASCT N	12
Median (P25-P75)	45.2 (25.9–54.6)
MDEs at trial entry‡	
SFLC ratio	51 (85)
>1 focal lesion MRI	22 (37)
>60% BM infiltration	21 (35)
Increased calcium	8 (13)
Renal failure	4 (7)
Anemia	19 (32)
Bone disease§	33 (55)
No. of MDEs present at entry	
1	11 (18)
2	16 (27)
3	33 (55)
ISS stage	
I	27 (45)
II	20 (33)
III	6 (10)
Unknown	7 (12)

Table 2 (*continues*)

Table 2 (*continued*): Participant Demographics and Laboratory Features

Parameter	Value
Laboratory markers‖	
β_2-microglobulin (n = 53)	2.8 (2.4–4.1)
Albumin (n = 54)	36.0 (32.0–39.0)
Plts (n = 56)	231.0 (190.5–274.0)
Hb (n = 56)	115.5 (102.0–132.5)
Calcium (n = 54)	2.3 (2.2–2.4)
LDH (n = 38)	164.5 (142.0–210.0)
Creatinine (n = 56)	77.5 (67.0–87.5)
Tumor assessments and genetics	
Translocations	
t (4,14)	3 (5)
t (14,16)	3 (5)
t (14,20)	1 (2)
t (11,14)	6 (10)
Abnormalities	
1p	3 (5)
1q	17 (28)
gain 11	15 (25)
del 17p	1 (2)
High risk (t [4,14], t [14,16], t [14,20], 1p, 1q, del17p)	20 (33)

Note.—Values shown as number with percent in parentheses or median with interquartile range in parentheses; age is shown as mean ± standard deviation. ASCT = autologous stem cell transplant, BM = bone marrow, Hb = hemoglobin, LDH = lactate dehydrogenase, MGUS = monoclonal gammopathy of uncertain significance, MM = multiple myeloma, Plts = platelets, SFLC = serum free light chain.
* Percentages of participants newly diagnosed.
† Percentages of participants relapsing at trial entry.
‡ Participants could present more than one myeloma-defining event (MDE).
§ Bone disease as per conventional imaging or prior to study entry.
‖ Number of participants shown who had blood markers available.

Discordance was significant for all regions ($P < .001$), demonstrating consistently higher sensitivity of WB-MRI for detection of diffuse disease.

Overall assessment.— WB-MRI was characterized by higher disease burden scores overall and for all sites than FDG PET/CT (Fig 7B, 7C, Table E3 [supplement]). The median total focal disease burden score for WB-MRI was 8.5 (IQR, 2.5–19) and was higher than that for FDG PET/CT, which had an average score of 4 (IQR, 0–9; $P < .001$). The concordance correlation index for total focal disease burden score was 0.583, indicating a low agreement (Fig 7C).

Clinical Implications of WB-MRI Disease Burden Sensitivity and Correlation with Traditional Quantitative Disease Markers

Among participants with a new diagnosis, 39% (17 of 44) showed two or more bone marrow focal lesions that were larger than 5 mm in size, constituting active disease as per IMWG diagnostic criteria. Of these, two were only identified with WB-MRI but not with FDG PET/CT. However, both participants also fulfilled at least one other of the IMWG criteria for active disease, such as abnormal serum free light chain ratio, and would have been classified as symptomatic regardless of findings at WB-MRI or FDG PET/CT.

We compared current routine direct (bone marrow infiltration) and surrogate quantitative (paraprotein) measures of disease with radiologic disease assessment to determine imaging capacity for disease burden assessment. Diagnostic bone marrow biopsy immediately before or after WB-MRI was available in 44 of 60 participants. Plasma cell infiltration (percentage of nucleated cells) by histopathologic analysis was higher (median, 60%; IQR, 50%–60.5%) in participants with diffuse disease detected at WB-MRI than for those without (median, 15%; IQR, 4%–50%; $P = .03$), whereas there was no evidence of a difference in infiltration between diffuse disease versus none at FDG PET/CT (Fig 8A; Table E4 [supplement]). Presence of focal disease alone at WB-MRI or FDG PET/CT did not correlate with the level of background bone marrow infiltration (Fig E1A [supplement]).

Serum paraprotein levels, which are used as surrogate markers of disease burden for diagnosis (9), were higher for participants with diffuse disease at WB-MRI (median, 32.0 g/L;

Table 3: Presence of Focal Disease at WB-MRI and/or FDG PET/CT and Association with Number of Lesions and Diffuse Disease

Parameter	Overall (n = 60)	Focal Lesions			P Value*
		WB-MRI(−) and FDG PET/CT(−) (n = 10)	WB-MRI(+) and FDG PET/CT(+) (n = 36)	WB-MRI(+) and FDG PET/CT(−) (n = 14)	
No. of focal lesions at WB-DWI					
No lesions	10 (17%)	10 (100%)	0	0	<.001
1–4	26 (43%)	0	15 (42%)	11 (79%)	
5–10	10 (17%)	0	9 (25%)	1 (7.1%)	
>10	14 (23%)	0	12 (33%)	2 (14%)	
Diffuse disease at MRI					
Yes	49 (82%)	10 (100%)	30 (83%)	9 (64%)	.08
No	11 (18%)	0	6 (17%)	5 (35%)	
Diffuse disease at PET					
Yes	10 (17%)	4 (40%)	6 (17%)	0	.03
No	50 (83%)	6 (60%)	30 (83%)	14 (100%)	
Diffuse disease					
MRI (−)/PET (−)	10 (17%)	0	5 (14%)	5 (36%)	.049
MRI (+)/PET (+)	9 (15%)	4 (40%)	5 (14%)	0	
MRI (+)/PET (−)	40 (67%)	6 (60%)	25 (69%)	9 (64%)	
MRI (−)/PET (+)	1 (1.7%)	0	1 (2.8%)	0	

Note.—FDG = fluorodeoxyglucose, FDG/PET(+) = lesion found at FDG/PET, FDG/PET(−) = no lesion found at FDG/PET, WB = whole body, WB-MRI(+) = lesion found at WB-MRI, WB-MRI(−) = no lesion found at WB-MRI.
* P value shown for an exact test.

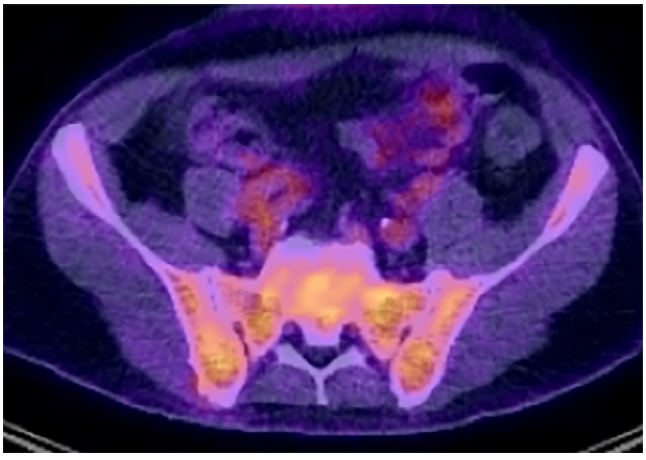

Figure 6: Image in a 59-year-old man shows diffuse disease at fluorodeoxyglucose (FDG) PET/CT. There is increased FDG uptake on fused PET/CT images relative to background tissues (80% bone marrow infiltration by myeloma cells; IgG κ paraprotein, 69 g/L; serum free κ light chains, 7 mg/L; λ light chains, 39 mg/L; light chain ratio, 0.02).

IQR, 24.0–48.0 g/L) compared with those without (median, 20.0 g/L; IQR, 12.0–22.6 g/L; P = .02). However, we found no evidence of a difference between paraprotein levels between participants who did or did not have diffuse disease at FDG PET/CT (Fig 8B; Table E4 [supplement]). Again, focal disease detection alone was not associated with paraprotein burden with either modality (Fig E1B [supplement]).

Association of Imaging Phenotypes with High-Risk Disease

High-risk genetic markers t(4;14), t(14;16), t(14;20), del(1p), gain(1q), and del(17p) were detected in 33% (20 of 60) of tumors. Of note, all high-risk tumors were characterized by diffuse disease infiltration at WB-MRI (Table E5 [supplement]). In particular, 70% (seven of 10) of participants who had no detectable focal disease with WB-MRI but did have diffuse infiltration at WB-MRI carried high-risk genetics, compared with 28% (11 of 40) of participants with focal lesions and diffuse infiltration (P = .03) detected at both WB-MRI and FDG PET/CT (Fig 8C).

Participants with WB-MRI diffuse disease without focal lesions (n = 9) had higher β_2-microglobulin values (median, 3.8 mg/L; IQR, 2.9–5.5 mg/L) than the overall group (median, 2.8 mg/L; IQR, 2.4–4.1 mg/L [Table 1]), as well as lower hemoglobin levels (95.0 g/L [IQR, 92.0–115.0 g/L] vs 115.5 g/L [IQR, 102–132.5 g/L]), indicative of clinically aggressive disease.

Discussion

We report prospectively collected results comparing WB-MRI as per the MY-RADS consensus (15) and FDG PET/CT for imaging assessment of myeloma. Using standardized image acquisition, predefined reporting standards, and blinded multiexpert reviews for both WB-MRI and FDG PET/CT, our results establish higher focal disease detection at WB-MRI with the exception of ribs, scapulae, clavicles, and cervical

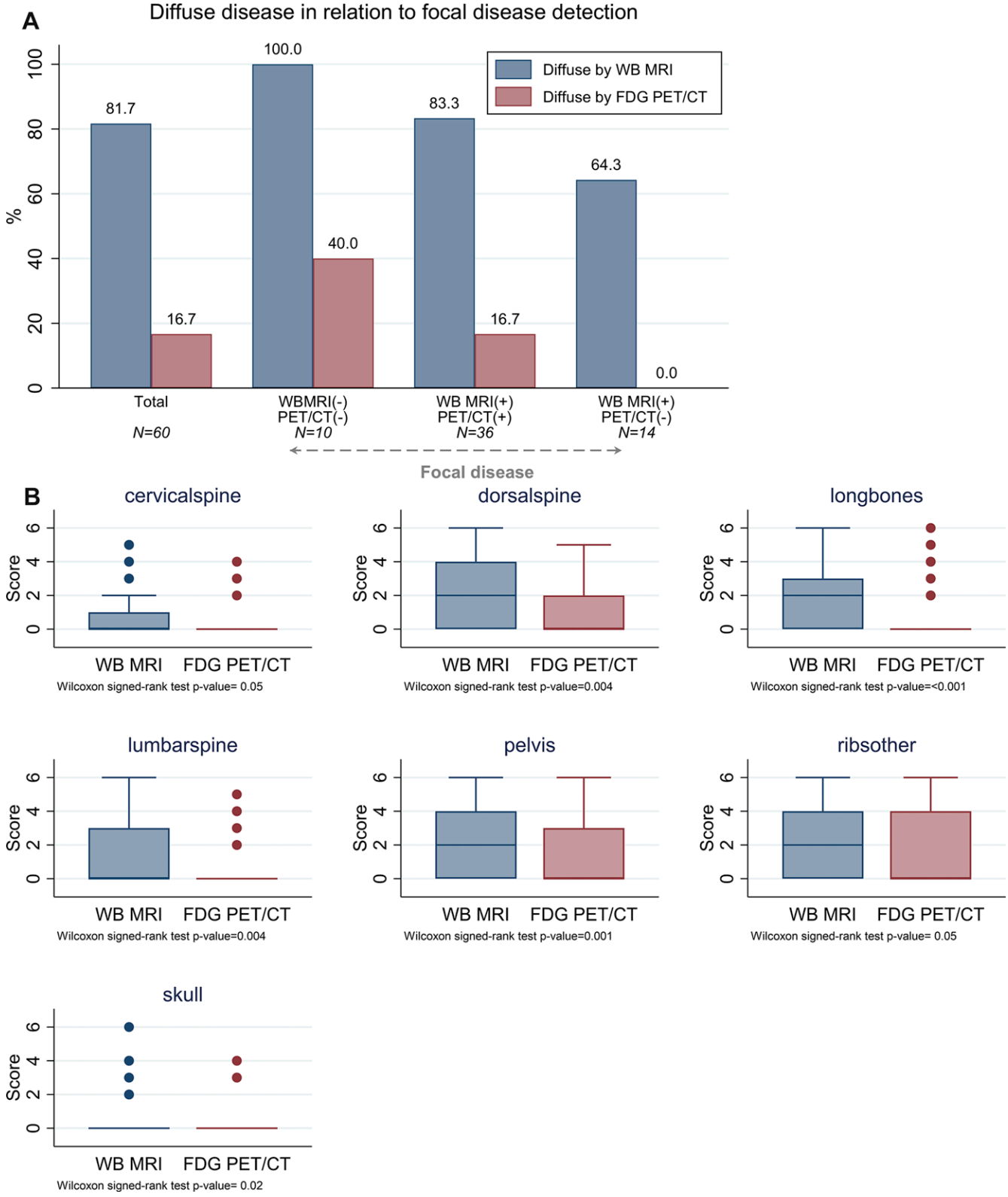

Figure 7: Disease burden scores per anatomic region and overall by whole-body (WB) MRI versus fluorine 18 fluorodeoxyglucose (FDG) PET/CT. **(A)** Bar chart shows diffuse disease detection in relation to detection of focal lesions. **(B)** Disease burden scores were calculated at WB-MRI and FDG PET/CT for all 60 participants for each anatomic region, as well as the total score for the entire imaged WB area. Box plots show median with the upper and lower quartiles and range of observed values. Differences in burden scores between WB-MRI and FDG PET/CT were significant for all anatomic regions ($P < .05$, adjusted by Holm multiplicity correction) and the total score ($P < .001$).***(Figure 7 continues)***

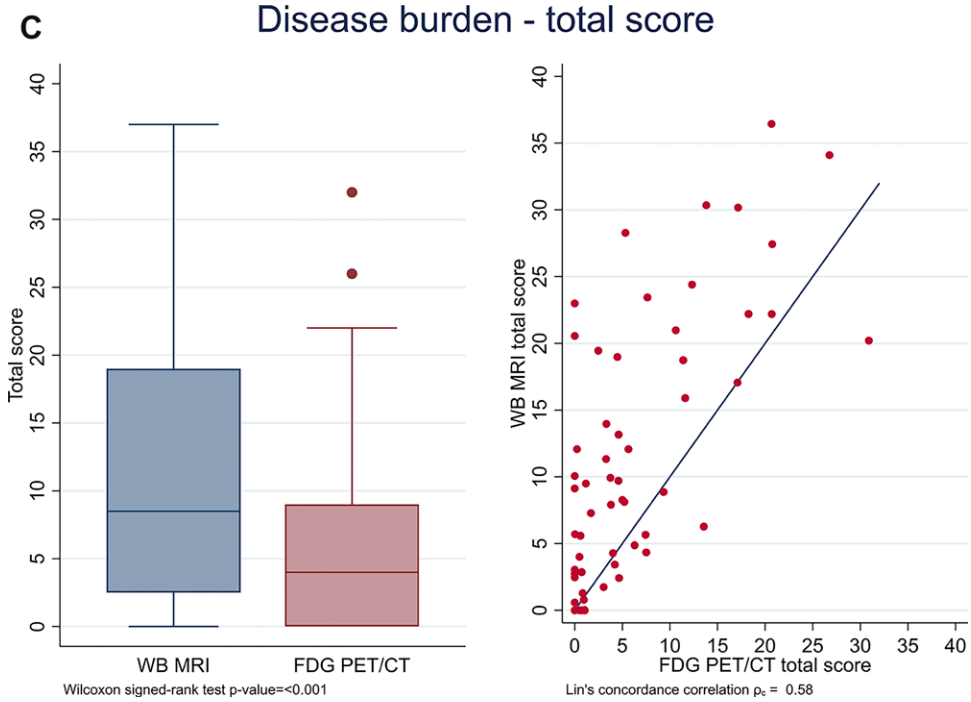

Figure 7 (*continued*): **(C)** The total disease burden score for the entire WB imaged area is summarized in boxplots for each imaging modality, which shows there were significant differences between WB-MRI and FDG PET/CT ($P < .001$). Dot plot shows agreement between WB-MRI and FDG PET/CT total disease burden score for individual participants.

spine, where detection was equivalent. Sensitivity of WB-MRI for detecting diffuse disease was significantly higher than that of FDG PET/CT for all bone marrow regions: Fewer than a quarter of tumors identified to have diffuse infiltration at WB-MRI were detected with FDG PET/CT, which is consistent with previous retrospective studies (17). Accordingly, total disease burden scores were consistently higher at WB-MRI than at FDG PET/CT. The high proportion of participants with coexisting focal disease and diffuse infiltration at WB-MRI is likely to reflect increased sensitivity for diffuse disease detection with WB-MRI techniques and that most participants have background diffuse infiltration, which is supported by trephine biopsy–proven diffuse bone marrow infiltration outside of focal areas of disease. We have also been able to report resolution of all additional focal lesions identified at WB-MRI compared with FDG PET/CT as evidence against false-positive findings. It has been postulated that a combination of advanced technical MRI capabilities and low expression of hexokinase-2 (which is involved in the glycolysis pathway) in some myeloma disease improves detection of disease at MRI over FDG PET/CT (28). It will be important to monitor emerging evidence that indicates that chemokine receptor 4–targeted PET/CT with gallium 68–Pentixafor or CD38-targeted PET/CT with zirconium 89-DFO-daratumumab may detect a higher number of myeloma lesions in the bone marrow compared with FDG PET/CT (29,30). PET/MRI may also be an important step forward in understanding the clinical relevance of differential lesion detection using different imaging techniques (31).

This study shows the importance of comparing imaging protocols for optimal disease detection and characterization. Approaches such as comparison of WB FDG PET/CT against standard MRI of the spine and pelvis without diffusion-weighted imaging have previously shown no difference in lesion detection (32). However, our analysis is in line with results reported for retrospective series and a recent prospective study (18) comparing WB-MRI with FDG PET/CT; our work and others' firmly support wider use of WB-MRI for myeloma (17,33). This is further supported by published evidence on high interobserver agreement in WB-MRI reporting (34,35), interpretation of potential false-positive findings, and established international consensus criteria (15), together positioning WB-MRI as a new imaging standard for myeloma. We also recently published an open access knowledge-sharing approach that supports wide implementation of standardized WB-MRI for patients with myeloma, outside of highly specialized centers (36). Furthermore, standardized WB-MRI for myeloma response assessment has already been successfully implemented in a multicenter clinical trial, OPTIMUM/MUKnine (ClinicalTrials.gov identifier NCT03188172).

In addition, we demonstrated a quantitative correlation between imaging disease assessment with WB-MRI and disease bone marrow infiltration percentage at histopathologic analysis, as well as paraprotein levels. Interestingly, although many participants showed diffuse infiltration at imaging, the majority were staged International Staging System (ISS) I or II. This finding is likely to reflect increased sensitivity for diffuse disease with WB-MRI, and the predominance of ISS I or II–staged participants will be influenced by the inclusion criterion of fitness for autologous stem cell transplantation. The lack of correlation between laboratory measures of disease burden and FDG PET/CT may reflect poor detection of the diffuse phenotype. These poor detection outcomes are increasingly relevant as the

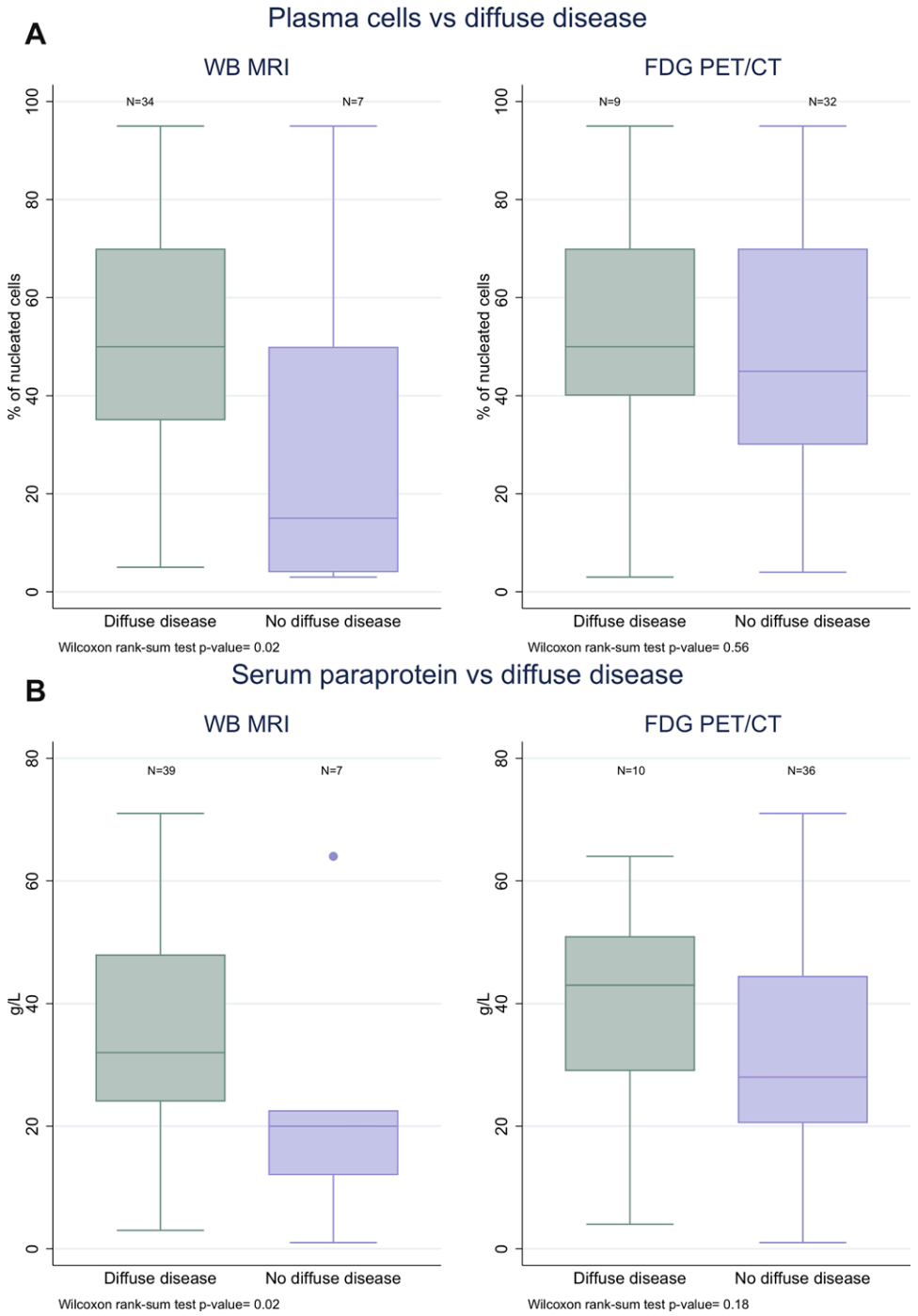

Figure 8: Relationship of whole-body (WB) MRI and fluorine 18 fluorodeoxyglucose (FDG) PET/CT with quantitative disease markers and patterns of disease at WB-MRI with genetic high-risk markers. **(A)** Plasma cell percentage (relative to nucleated bone marrow cells at histopathologic analysis) and **(B)** paraprotein levels were compared for groups with and without diffuse disease infiltration detected with WB-MRI or FDG PET/CT. Differences between those with diffuse disease versus those without were statistically significant for plasma cell percentage ($P = .03$) and paraprotein levels ($P = .02$) at WB-MRI but not at FDG PET/CT. ***(Figure 8 continues)***

role for imaging follow-up in patients with oligoclonal or nonsecretory disease grows and for surveillance strategies where repeated trephine biopsy is too invasive. Our results provide proof of principle that WB-MRI could allow for disease quantification with spatial resolution for advanced diagnosis, staging, and monitoring for personalized management (37). Projects using machine learning approaches for assisted WB-MRI imaging interpretation are currently underway and will likely facilitate adoption of this technology. Under current IMWG diagnostic criteria, two participants in our study showed two or more focal lesions that were larger than 5 mm only at WB-MRI but not FDG PET/CT. Although diagnosis of these participants in our trial would not have been impacted had they been imaged with FDG PET/CT only, increased sensitivity of WB-MRI may lead

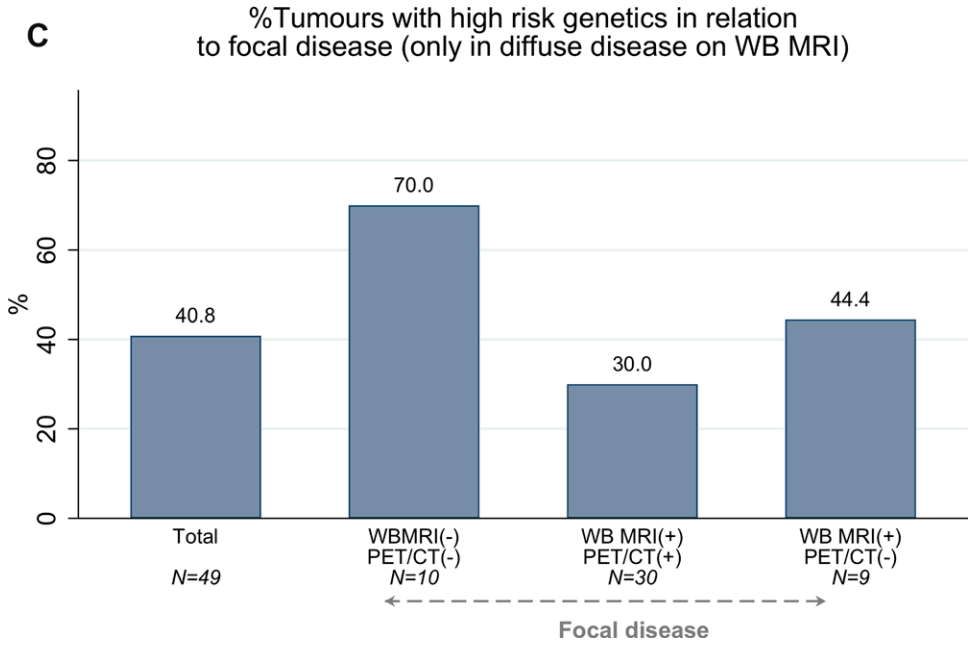

Figure 8 (*continued*): (C) Bar chart of participants with diffuse disease at WB-MRI show the percentage of tumors with high-risk genetics for the overall group, for participants without focal lesions, and for participants with focal lesions as detected with WB-MRI and/or FDG PET/CT. PET/CT(−) = participants without focal lesions at PET/CT, PET/CT(+) = participants with focal lesions at PET/CT, WB MRI(−) = participants without focal lesions at WB-MRI, WB MRI(+) = participants with focal lesions at WB-MRI.

to earlier detection of symptomatic disease in others. Patients can be treated without positive findings at imaging if laboratory parameters exceed levels defined in the IMWG criteria. Increased sensitivity of WB-MRI for detection of focal lesions will also have substantial impact for patients with asymptomatic myeloma at surveillance where small-volume disease detection is key, at restaging for confirmation of progression, and potentially for detecting posttherapy residual disease.

Beyond disease quantification, our results also suggest association of genetic and clinical high-risk disease with diffuse infiltration pattern at WB-MRI. In particular, more than two-thirds of tumors with diffuse infiltration but without focal lesions carried high-risk genetics, a finding that was underpinned by clinical characteristics of aggressive disease. Association of high-risk myeloma has been reported for diffuse infiltration at imaging, although in a retrospective series using conventional MRI imaging without diffusion-weighted imaging or Dixon imaging and restricted to imaging of the axial skeleton (38). Our results provide evidence for potential phenotypic prediction of high-risk disease with prospective standardized WB-MRI imaging. These findings advance the need to consider more accurate classification and diagnosis of the diffuse disease phenotype so that it can be explored further as a specific entity with consideration of implications for treatment. The negative implications of diffuse disease for patients have already been introduced by previous studies (38,39). Apparent diffusion coefficient thresholds for diagnosis of diffuse infiltration have been proposed (40), although these are potentially prone to bias from different MRI systems and effects from previous treatment. As preliminary evidence suggests that diffuse myeloma infiltration is relatively homogeneous (41), absence of focal lesions at sensitive WB-MRI and a positive finding at trephine biopsy could be used to classify the diffuse phenotype.

Specifically, in the context of myeloma, WB-MRI is well tolerated (17), and avoidance of radiation has been shown to be influential in directing patient preference for WB-MRI in patients with lung and colorectal cancers, although time to diagnosis and accuracy were more highly valued (42). The coverage and sensitivity of WB-MRI can raise concern regarding incidental findings. However, although incidental findings are common (38%), because tissue characterization is a strength of WB-MRI, only 3% result in a need for further investigation (43). WB-MRI does generate large data sets, which presents a substantial workload for radiologists. It is likely that WB-MRI reads will ultimately be supported by algorithms that facilitate detection of abnormal findings. Health economic evidence also supports adoption of WB-MRI because although up-front costs are higher than those of low-dose CT, the additional benefits result in an equivalent net monetary benefit compared with a negative net monetary benefit for FDG PET/CT (13).

Our study is limited by lack of outcome data and lack of per-lesion histopathologic analysis correlation. However, follow-up of the WB-MRI participant trial cohort is currently ongoing, and association with survival will be reported in a separate report when data are mature. Furthermore, the inclusion criteria defined that all participants had multiple myeloma requiring treatment, thereby limiting participants with a lower disease burden where WB-MRI would be most likely to alter decision to treat.

In summary, our results propose WB-MRI as a new standard for myeloma tumor imaging and supports its wider implementation in standard care as well as clinical research for the benefit of patients.

Data sharing: Data generated or analyzed during the study are available from the corresponding author by request.

Acknowledgments: We thank Alison Bonner, BS, Rebecca Cox, BS, and Leonora Conneely, BS, for their study support and Frances Aldridge and Julie Howard-Reeves for their cytogenetic expertise.

Author contributions: Guarantors of integrity of entire study, C.M., C.K.; study concepts/study design or data acquisition or data analysis/interpretation, all authors; manuscript drafting or manuscript revision for important intellectual content, all authors; approval of final version of submitted manuscript, all authors; agrees to ensure any questions related to the work are appropriately resolved, all authors; literature research, C.M., B.S., C.K., M.B., W.J.G.O., M.F.K.; clinical studies, C.M., D.L., K.B., C.P., A.R., K.D., J.C., V.M., S.S., C.K., P.K., J.W., M.B., W.J.G.O., M.F.K.; statistical analysis, N.P., C.K.; and manuscript editing, C.M., N.P., B.S., D.L., D.M.K., K.B., C.P., A.R., K.D., J.C., S.S., B.C., C.K., J.W., M.B., W.J.G.O., M.F.K.

Disclosures of Conflicts of Interest: **C.M.** disclosed no relevant relationships. **N.P.** disclosed no relevant relationships. **B.S.** disclosed no relevant relationships. **D.L.** disclosed no relevant relationships. **D.M.K.** disclosed no relevant relationships. **K.B.** received payment or honoraria for lectures, presentations, speakers bureaus, manuscript writing, or educational events from Celgene, Janssen, Sanofi, Novartis, and Takeda; received payment for expert testimony from Celgene, Takeda, Sanofi, and Janssen; received support for attending meetings and/or travel from Janssen, Celgene, Takeda, and GSK. **C.P.** received consulting fees from Amgen, Celgene, Janssen, Oncopeptides, and Sanofi; received payment or honoraria for lectures, presentations, speakers bureaus, manuscript writing, or educational events from Amgen, Jenssen, and Sanofi; received support for attending meetings and/or travel from Celgene, Janssen, and Amgen. **A.R.** disclosed no relevant relationships. **K.D.** disclosed no relevant relationships. **J.C.** disclosed no relevant relationships. **V.M.** disclosed no relevant relationships. **S.S.** disclosed no relevant relationships. **B.C.** disclosed no relevant relationships. **C.K.** disclosed no relevant relationships. **P.K.** disclosed no relevant relationships. **J.W.** disclosed no relevant relationships. **M.B.** has U.S. patent 10,885,679 (2021). **W.J.G.O.** disclosed no relevant relationships. **M.F.K.** disclosed no relevant relationships.

References

1. Hillengass J, Fechtner K, Weber MA, et al. Prognostic significance of focal lesions in whole-body magnetic resonance imaging in patients with asymptomatic multiple myeloma. J Clin Oncol 2010;28(9):1606–1610.
2. Kastritis E, Terpos E, Moulopoulos L, et al. Extensive bone marrow infiltration and abnormal free light chain ratio identifies patients with asymptomatic myeloma at high risk for progression to symptomatic disease. Leukemia 2013;27(4):947–953.
3. Merz M, Hielscher T, Wagner B, et al. Predictive value of longitudinal whole-body magnetic resonance imaging in patients with smoldering multiple myeloma. Leukemia 2014;28(9):1902–1908.
4. Moulopoulos LA, Gika D, Anagnostopoulos A, et al. Prognostic significance of magnetic resonance imaging of bone marrow in previously untreated patients with multiple myeloma. Ann Oncol 2005;16(11):1824–1828.
5. Moulopoulos LA, Dimopoulos MA, Smith TL, et al. Prognostic significance of magnetic resonance imaging in patients with asymptomatic multiple myeloma. J Clin Oncol 1995;13(1):251–256.
6. Mariette X, Zagdanski AM, Guermazi A, et al. Prognostic value of vertebral lesions detected by magnetic resonance imaging in patients with stage I multiple myeloma. Br J Haematol 1999;104(4):723–729.
7. Dhodapkar MV, Sexton R, Waheed S, et al. Clinical, genomic, and imaging predictors of myeloma progression from asymptomatic monoclonal gammopathies (SWOG S0120). Blood 2014;123(1):78–85.
8. Mateos MV, Hernández MT, Giraldo P, et al. Lenalidomide plus dexamethasone for high-risk smoldering multiple myeloma. N Engl J Med 2013;369(5):438–447.
9. Rajkumar SV, Dimopoulos MA, Palumbo A, et al. International Myeloma Working Group updated criteria for the diagnosis of multiple myeloma. Lancet Oncol 2014;15(12):e538–e548.
10. Dimopoulos M, Terpos E, Comenzo RL, et al. International myeloma working group consensus statement and guidelines regarding the current role of imaging techniques in the diagnosis and monitoring of multiple Myeloma. Leukemia 2009;23(9):1545–1556.
11. Dimopoulos MA, Hillengass J, Usmani S, et al. Role of magnetic resonance imaging in the management of patients with multiple myeloma: a consensus statement. J Clin Oncol 2015;33(6):657–664.
12. Hillengass J, Usmani S, Rajkumar SV, et al. International myeloma working group consensus recommendations on imaging in monoclonal plasma cell disorders. Lancet Oncol 2019;20(6):e302–e312.
13. NICE Guideline on Myeloma: diagnosis and management. UK National Institute for Health and Care Excellence. https://www.nice.org.uk/guidance/ng35. Accessed June 12, 2020.
14. Gariani J, Westerland O, Natas S, Verma H, Cook G, Goh V. Comparison of whole body magnetic resonance imaging (WBMRI) to whole body computed tomography (WBCT) or 18F-fluorodeoxyglucose positron emission tomography/CT (18F-FDG PET/CT) in patients with myeloma: Systematic review of diagnostic performance. Crit Rev Oncol Hematol 2018;124:66–72.
15. Messiou C, Hillengass J, Delorme S, et al. Guidelines for acquisition, interpretation, and reporting of whole-body MRI in myeloma: Myeloma response assessment and diagnosis system (MY-RADS). Radiology 2019;291(1):5–13.
16. Sachpekidis C, Mosebach J, Freitag MT, et al. Application of (18)F-FDG PET and diffusion weighted imaging (DWI) in multiple myeloma: comparison of functional imaging modalities. Am J Nucl Med Mol Imaging 2015;5(5):479–492.
17. Pawlyn C, Fowkes L, Otero S, et al. Whole-body diffusion-weighted MRI: a new gold standard for assessing disease burden in patients with multiple myeloma? Leukemia 2016;30(6):1446–1448.
18. Westerland O, Amlani A, Kelly-Morland C, et al. Comparison of the diagnostic performance and impact on management of 18F-FDG PET/CT and whole-body MRI in multiple myeloma. Eur J Nucl Med Mol Imaging 2021;48(8):2558–2565.
19. Bartel TB, Haessler J, Brown TL, et al. F18-fluorodeoxyglucose positron emission tomography in the context of other imaging techniques and prognostic factors in multiple myeloma. Blood 2009;114(10):2068–2076.
20. Latifoltojar A, Boyd K, Riddell A, Kaiser M, Messiou C. Characterising spatial heterogeneity of multiple myeloma in high resolution by whole body magnetic resonance imaging: Towards macro-phenotype driven patient management. Magn Reson Imaging 2021;75:60–64.
21. Sonneveld P, Avet-Loiseau H, Lonial S, et al. Treatment of multiple myeloma with high-risk cytogenetics: a consensus of the International Myeloma Working Group. Blood 2016;127(24):2955–2962.
22. Rasche L, Chavan SS, Stephens OW, et al. Spatial genomic heterogeneity in multiple myeloma revealed by multi-region sequencing. Nat Commun 2017;8(1):268.
23. Yu Y, Brown Wade N, Hwang AE, et al. Variability in cytogenetic testing for multiple myeloma: A comprehensive analysis from across the United States. JCO Oncol Pract 2020;16(10):e1169–e1180.
24. Durie BG, Harousseau JL, Miguel JS, et al. International uniform response criteria for multiple myeloma. Leukemia 2006;20(9):1467–1473 [Published corrections appear in Leukemia 2006;20(12):2220 and Leukemia 2007;21(5):1134.].
25. Giles SL, Messiou C, Collins DJ, et al. Whole-body diffusion-weighted MR imaging for assessment of treatment response in myeloma. Radiology 2014;271(3):785–794.
26. Nanni C, Cottereau AS, Lopci E, et al. Report of the 6th International Workshop on PET in lymphoma. Leuk Lymphoma 2017;58(10):2298–2303.
27. Barrington SF, Mikhaeel NG, Kostakoglu L, et al. Role of imaging in the staging and response assessment of lymphoma: consensus of the International Conference on Malignant Lymphomas Imaging Working Group. J Clin Oncol 2014;32(27):3048–3058 [Published correction appears in J Clin Oncol 2016;34(21):2562.].
28. Rasche L, Angtuaco E, McDonald JE, et al. Low expression of hexokinase-2 is associated with false-negative FDG-positron emission tomography in multiple myeloma. Blood 2017;130(1):30–34.
29. Pan Q, Cao X, Luo Y, Li J, Feng J, Li F. Chemokine receptor-4 targeted PET/CT with 68Ga-Pentixafor in assessment of newly diagnosed multiple myeloma: comparison to 18F-FDG PET/CT. Eur J Nucl Med Mol Imaging 2020;47(3):537–546.
30. Ulaner GA, Sobol NB, O'Donoghue JA, et al. CD38-targeted Immuno-PET of Multiple Myeloma: From Xenograft Models to First-in-Human Imaging. Radiology 2020;295(3):606–615.
31. Mayerhoefer ME, Archibald SJ, Messiou C, Staudenherz A, Berzaczy D, Schöder H. MRI and PET/MRI in hematologic malignancies. J Magn Reson Imaging 2020;51(5):1325–1335.
32. Moreau P, Attal M, Caillot D, et al. Prospective evaluation of magnetic resonance imaging and [18F]fluorodeoxyglucose positron emission tomography-computed tomography at diagnosis and before maintenance therapy in symptomatic patients with multiple myeloma included in the IFM/DFCI 2009 Trial: Results of the IMAJEM study. J Clin Oncol 2017;35(25):2911–2918.
33. Chen J, Li C, Tian Y, et al. Comparison of whole-body DWI and 18F-FDG PET/CT for detecting intramedullary and extramedullary lesions in multiple myeloma. AJR Am J Roentgenol 2019;213(3):514–523.
34. Lai AYT, Riddell A, Barwick T, et al. Interobserver agreement of whole-body magnetic resonance imaging is superior to whole-body computed tomography

for assessing disease burden in patients with multiple myeloma. Eur Radiol 2020;30(1):320–327.
35. Lecouvet FE, Boyadzhiev D, Collette L, et al. MRI versus 18F-FDG-PET/CT for detecting bone marrow involvement in multiple myeloma: diagnostic performance and clinical relevance. Eur Radiol 2020;30(4):1927–1937.
36. Kaiser MF, Boyd K, Koh DM, Rata M, Blackledge M, Messiou C. Improving real-world myeloma patient access to whole body MRI through "open-access" knowledge sharing: The UK experience. eJHaem 2020;1(1):361–363.
37. Hill E, Turkbey B, Turkbey E, et al. Evaluation of whole-body MRI (WB-MRI) in smoldering multiple myeloma (SMM). Blood 2020;136(Supplement 1):19–20.
38. Moulopoulos LA, Dimopoulos MA, Kastritis E, et al. Diffuse pattern of bone marrow involvement on magnetic resonance imaging is associated with high risk cytogenetics and poor outcome in newly diagnosed, symptomatic patients with multiple myeloma: a single center experience on 228 patients. Am J Hematol 2012;87(9):861–864.
39. Mai EK, Hielscher T, Kloth JK, et al. A magnetic resonance imaging-based prognostic scoring system to predict outcome in transplant-eligible patients with multiple myeloma. Haematologica 2015;100(6):818–825.
40. Koutoulidis V, Fontara S, Terpos E, et al. Quantitative diffusion-weighted imaging of the bone marrow: An adjunct tool for the diagnosis of a diffuse MR imaging pattern in patients with multiple myeloma. Radiology 2017;282(2):484–493.
41. Keeling A, O'Connor S, Boyd K, et al. Lack of clinically meaningful anatomical variations in bone marrow apparent diffusion coefficient in diffuse pattern myeloma allows untargeted sampling to confirm disease burden. J Radiol Imaging 2020;4(4):25–29.
42. Miles A, Taylor SA, Evans REC, et al. Patient preferences for whole-body MRI or conventional staging pathways in lung and colorectal cancer: a discrete choice experiment. Eur Radiol 2019;29(7):3889–3900.
43. Wale A, Pawlyn C, Kaiser M, Messiou C. Frequency, distribution and clinical management of incidental findings and extramedullary plasmacytomas in whole body diffusion weighted magnetic resonance imaging in patients with multiple myeloma. Haematologica 2016;101(4):e142–e144.